

## A Hydrophobicity Scale for the Lipid Bilayer Barrier Domain from Peptide Permeabilities: Nonadditivities in Residue Contributions<sup>†</sup>

Peter Terry Mayer,<sup>‡</sup> Tian-Xiang Xiang,<sup>§</sup> Riku Niemi,<sup>||</sup> and Bradley D. Anderson<sup>\*,§</sup>

Department of Pharmaceutics and Pharmaceutical Chemistry, University of Utah, Salt Lake City, Utah 84108, and Division of Pharmaceutical Sciences, College of Pharmacy, University of Kentucky, Lexington, Kentucky 40515

Received August 21, 2002; Revised Manuscript Received December 4, 2002

**ABSTRACT:** Passive peptide transport across lipid membranes is governed by the energetics of partitioning into the ordered chain interior coupled with the rate of diffusion across this region. A hydrophobicity scale for peptide transfer into the barrier region of membranes derived from permeability coefficients would be useful to predict passive permeation of peptides across biomembranes and for determining the thermodynamics of peptide/protein insertion into the membrane interior. This study reports transport rates across large unilamellar vesicles (LUVs) composed of egg lecithin at 25 °C for a series of peptides having the general structure N-*p*-toluyl-(X)<sub>*n*</sub> (*n* = 1–3), where X is glycine, alanine, or sarcosine. Apparent residue group contributions were calculated from permeability coefficients, *P*<sub>RX</sub>, using the equation  $\Delta(\Delta G^\circ)_X = -RT \ln(P_{RX}/P_{RH})$ . Multiple linear least-squares regression analysis performed for the set of 14 permeants yielded the best correlation (*r*<sup>2</sup> = 0.9993) when the following permeant descriptors were utilized: side-chain nonpolar surface area, number of –CONH– residues, number of toluyl-CON(Me)– residues, and number of other –CON(Me)– residues. The backbone –CONH– residue contribution in peptides, 4.6 kcal/mol, is significantly lower than that obtained for a single isolated –CONH– (>6 kcal/mol), suggesting a possible influence of intramolecular hydrogen bonding. Under closer scrutiny,  $\Delta(\Delta G^\circ)_X$  for the Ala and Gly residues decrease with increasing peptide length. The effect of *N*-methylation is also highly dependent on position and number of *N*-methyl groups on the molecule ( $\Delta(\Delta G^\circ)_X = -0.5$  to  $-2.2$  kcal/mol). These nonadditivities may be rationalized by considering the effects of peptide length and *N*-methylation on membrane-induced intramolecular hydrogen bonding leading to various folded conformations.

A quantitative understanding of the thermodynamics of peptide partitioning and folding in various regions of lipid membranes is important in unraveling the membrane affinity of a variety of membrane-active peptides and membrane proteins, and the mechanisms by which they perform their biological function. Such information would also be useful in developing reliable methods for the computational prediction of membrane transport properties of pharmacologically active peptides and peptidomimetics, an area that is becoming increasingly important in drug discovery as the number of drug candidates emerging from various high-throughput screens continues to escalate.

The overall free energy for insertion of a peptide or protein into the hydrocarbon core of a membrane can be viewed thermodynamically in terms of two distinct events: (a) the

free energy change accompanying the transfer of the fully extended peptide from water into the hydrocarbon interior,  $\Delta G_{w \rightarrow hc}$ ; and (b) intramolecular hydrogen bond formation,  $\Delta G_{\text{folding}}$ , leading to helix formation in peptides of sufficient length. We are interested in the energies governing both of these processes. Although this thermodynamic cycle is attractive for its conceptual simplicity, experimental determination of the energies associated with each of the above processes has proven to be far from simple. Traditionally, free energies of transfer of model compounds varying in a single amino acid residue or amino acid side chain from water into various bulk organic solvents have served as a basis for estimating individual residue contributions (i.e., solvation parameters) to the overall transfer free energy for fully extended peptides or proteins from water into membranes. Transfer free energies based on octanol/water partition coefficients are most common (1–4), but several labs have correctly noted that  $\Delta G_{\text{transfer}}^\circ$  values vary significantly, depending on the nature of the nonaqueous solvent into which the transfer occurs (5, 6). Recently, White and co-workers have defined a hydrophobicity scale for binding of peptides at the bilayer interface based on equilibrium partition coefficients of small peptides between aqueous solution and DMPC or POPC bilayers (7–9). They observed a “remarkable correlation” between interfacial hydrophobicity and that of octanol, with a slope of approximately 0.5 when the solvation parameters for interfacial binding were plotted

<sup>†</sup> Work funded by NIH Grant RO1 GM51347. Peter Mayer was also supported by an Advanced Predoctoral Fellowship from the Pharmaceutical Research and Manufacturers of America Foundation (PhRMA). Riku Niemi was financially supported through fellowships from the Academy of Finland, the Finnish Cultural Foundation, the Saastamoinen Foundation, the Magnus Ehrnrooth Foundation, the University of Kuopio, and thanks to Scandinavia, Inc.

\* Corresponding author.

<sup>‡</sup> Currently at Whitehall-Robins Healthcare Corporation, 1211 Sherwood Ave., Richmond, VA 23220.

<sup>§</sup> Currently at the University of Kentucky, Division of Pharmaceutical Sciences, College of Pharmacy, Lexington, KY 40515.

<sup>||</sup> Currently at the University of Kuopio, Kuopio, Finland.

<sup>1</sup> Abbreviations: LUV, large unilamellar vesicle; Tol, *p*-toluyl-; SAR, sarcosine; *P*, permeability coefficient.

against those for octanol/water partitioning. While they pointed out that the interface is chemically heterogeneous and no unique hydrophobicity scale could account for the depth dependent properties of this region, the interfacial region clearly permits substantial hydrogen bonding to the polar peptide residues. On the basis of the fact that the peptides chosen for their investigations remain fully extended on binding, the interfacial hydrophobicity scale of Wimley and White provides the free energy for interfacial binding of the unfolded peptide (9).

Quantifying the thermodynamic parameters governing peptide or protein transfer from water to the hydrocarbon core of a membrane poses a more difficult problem. The energetic cost for partitioning a peptide bond ( $-\text{CONH}-$ ) into the hydrocarbon core has been estimated to be 6.12 kcal/mol by Roseman (10) from the partitioning of *N*-methylacetamide from water to  $\text{CCl}_4$  corrected by the fragmental constants for the  $\text{N}-\text{CH}_3$  and  $\alpha\text{-CH}_3$  groups. This substantial energetic cost can be significantly reduced by intramolecular hydrogen bonding leading to helix formation in large peptides, a process referred to as partitioning-folding coupling (8). Though clearly important, the energy per residue gained from helix formation is a matter of controversy (11). As pointed out by White and Wimley (9), accurate experimental values for the energetics of  $-\text{CONH}-$  partitioning and hydrogen bond formation are crucial for predicting membrane helices in hydropathy plot analyses in addition to their value in predicting peptide drug permeabilities.

Previous membrane transport experiments have established that the bilayer barrier domain resides within the ordered acyl chain region of lipid bilayers, the selectivity of which to variations in permeant polarity resembles that of a nonpolar hydrocarbon solvent such as 1,9-decadiene (for egg PC) (12, 13) or hexadecane (for DPPC) (14). The effects of several well-isolated functional groups attached to *p*-toluic acid and *p*-methylhippuric acid on permeability have been shown to be independent of the molecule to which the substituent is attached. Assuming that diffusivity is approximately constant, a reasonable assumption for molecules having similar minimum cross-sectional surface areas (14), one can derive apparent  $\Delta(\Delta G^\circ)_X$  values representing the substituent's contribution to the free energy of transfer into the barrier domain from the ratio of permeability coefficients for the substituted ( $P_{\text{RX}}$ ) to the unsubstituted reference compound ( $P_{\text{RH}}$ ), as described in eq 1:

$$\Delta(\Delta G^\circ)_X = -RT \ln \left( \frac{P_{\text{RX}}}{P_{\text{RH}}} \right) \quad (1)$$

These  $\Delta(\Delta G^\circ)_X$  values offer the means for generating a new hydrophobicity scale representing the selectivity of the ordered hydrocarbon core of lipid bilayers, a region that cannot be easily probed in equilibrium partitioning experiments which either sample the interfacial region at various immersion depths (7, 8, 15, 16) or, when a transmembrane location can be demonstrated (17, 18), yield free energies composed of several contributions including  $\Delta G_{\text{w} \rightarrow \text{hc}}$ ,  $\Delta G_{\text{folding}}$ , plus possible interfacial contributions and uncorrected effects of conformation or aggregation in the aqueous phase and are thus very difficult to interpret.

This report extends our previous bilayer transport studies to a series of glycine- (G), alanine- (A), and sarcosine- (SAR)

containing peptides of *p*-toluic acid (TOL- $G_n$ , TOL- $A_m$ , TOL-Sar $_m$ - $G_n$ -SAR), where  $n = 0-3$ ,  $m = 0-2$ , and  $l = 0-2$ . These small peptides have the likely advantage of being predominantly in their random coil state in aqueous solution and are limited in terms of the folded conformations that they can adopt in the bilayer interior due to their size. Since portions of the backbone or side chain residues in a peptide may not be fully exposed to the solvent even in fully extended peptides due to occlusion by neighboring side chains, atomic solvation parameters are typically normalized to solvent-accessible surface areas (1, 2, 19). We have adopted this approach to determine the solvation parameter for nonpolar residues in the bilayer interior using nonpolar residue accessible surface areas obtained from an AcGG-X-GG peptide as reported by Wimley et al. (19).

A dynamic equilibrium exists between unfolded and extended structures even in relatively small peptides with folded structures being favored in nonpolar solvents (similar to the environment within the barrier domain). Thus, intramolecularly H-bonded  $C_7$  conformers of AcProNHMe dominate in nonpolar solvents (20), while tripeptide amides (e.g., *N*-acetyl-L-Pro-L-Leu-Gly-NH<sub>2</sub>) exhibit  $3 \rightarrow 1$  and  $4 \rightarrow 1$  intramolecular H-bonds corresponding to 10-membered and 13-membered rings resembling  $\beta$ -turns and  $\alpha$ -helices common in polypeptide chains (21, 22). Folded  $\beta$ I type turns have been implicated in the unusual blood-brain barrier permeability of the  $\delta$ -sleep-inducing peptide, an endogenous charged, hydrophilic nonapeptide (23). Nonadditivity in the peptide bond contribution may occur with increasing peptide length due to shifts in conformational states as additional peptide residues are added allowing more secondary structure. The effects of *N*-methylation on peptide affinity for the bilayer interior are of particular interest. The removal of potential H-bonding sites through *N*-methylation increases the intrinsic lipophilicity of the peptide bond but may also reduce intramolecular hydrogen-bonding and alter the distribution of folded conformational states. Certainly intramolecularly H-bonded species may be further diminished in *N*-methylated peptides due to their significant populations of cis isomers (24). These subtle effects are revealed in a substantial dependence of the  $\Delta(\Delta G^\circ)_X$  for *N*-methylation on the position and number of such substituents in the model peptides explored.

## EXPERIMENTAL PROCEDURES

**Materials.** Egg lecithin-phosphatidylcholine (egg-PC, >99%) and phosphatidic acid (egg-PA, >99%) were obtained from Avanti Polar-Lipids, Inc. (Pelham, AL). All commercially obtained reagents were used as received. Any peptides used as permeants in these experiments that were not commercially available were synthesized as described below. Preparative scale HPLC was performed using a C-18 column (Partisil 10, ODS-3, 25.4 mm i.d.  $\times$  300 mm, Whatman, Fairfield, NJ) with acetonitrile:water varying from 10% to 20% organic at a flow rate of 5.0 mL/min. The aqueous phase for the preparative scale HPLC was pure water with the pH adjusted to 3.0 using HCl.

*p*-Toluyldiglycine (Tol-G-G, [2-(4-methyl-benzoylamino)-acetylaminol]-acetic acid) was synthesized by the Department of Medicinal Chemistry, University of Utah, using a standard F-MOC solid-phase chemistry synthetic procedure and was

used as received.  $^1\text{H}$  NMR ( $\text{D}_2\text{O}$ ):  $\delta$  7.64 (d, 2H, *o*), 7.28 (d, 2H, *m*), 4.05 (s, 2H,  $\text{CH}_2$ ), 3.80 (s, 2H,  $\text{CH}_2$ ), and 2.31 (s 3H, *p*- $\text{CH}_3$ ). The mass spectrum was consistent with the indicated structure, having a parent ion peak at  $m/z = 250$ . Purity was >95% by HPLC.

*p*-Toluyltriglycine (Tol-G-G-G, {2-[2-(4-methyl-benzoylamino)-acetyl]amino}-acetyl) was synthesized by the Department of Medicinal Chemistry, University of Utah, using a standard F-MOC solid-phase chemistry procedure and was used as received.  $^1\text{H}$  NMR ( $\text{D}_2\text{O}$ ):  $\delta$  7.64 (d, 2H, *o*), 7.28 (d, 2H, *m*), 4.06 (s, 2H,  $\text{CH}_2$ ), 3.91 (s, 2H,  $\text{CH}_2$ ), 3.73 (s, 2H,  $\text{CH}_2$ ) and 2.31 (s 3H, *p*- $\text{CH}_3$ ). The mass spectrum was consistent with the indicated structure, having a parent ion peak at  $m/z = 307$ . Purity was >95% by HPLC.

*p*-Toluyllalanine (Tol-A, 2-(4-methyl-benzoylamino)-propionic acid) was synthesized by dissolving *p*-toluic acid (2.0 g) into 20 mL of dry DMF in a vessel sealed to prevent exposure to water vapor. The solution was cooled to  $<-10^\circ\text{C}$  in an acetone/liquid nitrogen bath and a 20% molar excess each of diisopropylethylamine and isobutyl chloroformate were added. The solution was allowed to react for 10 min with gentle agitation. The reaction flask was then transferred to an ice water bath, and 2 equiv of an aqueous solution of alanine (1.25 M @ pH 10.5, adjusted w/NaOH) were added and allowed to react for 10 min. The reaction product, Tol-A, was isolated by the preparative scale HPLC method described above. The product was dried in vacuo, yielding 1.2 g of needle shaped crystals.  $^1\text{H}$  NMR ( $\text{D}_2\text{O}$ ):  $\delta$  7.60 (d, 2H, *o*), 7.25 (d, 2H, *m*), 4.41 (q, 1H, CH), 2.30 (s, 3H, *p*- $\text{CH}_3$ ) and 1.41 (d, 3H,  $-\text{CH}_3$ ). The mass spectrum was consistent with the indicated structure, having a parent ion peak at  $m/z = 207$ . Purity was >99% by HPLC.

*p*-Toluyldialanine (Tol-A-A, 2-[2-(4-methyl-benzoylamino)-propionylamino]-propionic acid) was synthesized by dissolving *p*-toluic acid (0.2 g) in 4 mL of dry DMF in a vessel sealed to prevent exposure to water vapor. The procedure was the same as above for synthesis of Tol-A, but the aqueous dialanine reactant solution was 1.75 M at pH 10.2. The reaction product, Tol-AA, was isolated by preparative HPLC as above. The product was dried in vacuo then recrystallized from warm acetonitrile, yielding 0.14 g of platelike birefringent crystals.  $^1\text{H}$  NMR ( $\text{D}_2\text{O}$ ):  $\delta$  7.60 (d, 2H, *o*), 7.25 (q, 2H, *m*), 4.40 (q, 1H, CH), 4.27 (q, 1H, CH), 2.29 (s, 3H, *p*- $\text{CH}_3$ ), 1.38 (d, 3H,  $-\text{CH}_3$ ), and 1.33 (d, 3H,  $-\text{CH}_3$ ). The mass spectrum was consistent with the indicated structure, having a parent ion peak at  $m/z = 278$ . Purity was >99% by HPLC.

*p*-Toluyltrialanine (Tol-AAA, 2-{2-[2-(4-methyl-benzoylamino)-propionylamino]-propionylamino}-propionic acid) was synthesized by dissolving *p*-toluic acid (0.1 g) into 3 mL of dry DMF in a vessel sealed to prevent exposure to water vapor. The synthetic procedure was the same as for Tol-A, but 1.5 equiv of trialanine were added as an aqueous solution (0.6 M at pH 10.0). The reaction product, Tol-AAA, was isolated by preparative scale HPLC as above. The combined product from two such syntheses was dried in vacuo and then recrystallized from methanol/water in a freezer, yielding 0.2 g of platelike birefringent crystals.  $^1\text{H}$  NMR ( $\text{D}_2\text{O}$ ):  $\delta$  7.60 (d, 2H, *o*), 7.25 (q, 2H, *m*), 4.38 (q, 1H, CH), 4.25 (q, 1H, CH), 4.19 (q, 1H, CH), 2.30 (s, 3H, *p*- $\text{CH}_3$ ), 1.39 (d, 3H,  $-\text{CH}_3$ ), 1.31 (d, 3H,  $-\text{CH}_3$ ), and 1.29 (d, 3H,  $-\text{CH}_3$ ). The mass spectrum was consistent with the

indicated structure, having a parent ion peak at  $m/z = 349$ . Purity was >99% by HPLC.

*p*-Toluylsarcosine (Tol-SAR, [methyl-(4-methyl-benzoyl)-amino]-acetic acid), *p*-toluyglycylsarcosine (Tol-G-SAR, {methyl-[2-(4-methyl-benzoylamino)-acetyl]-amino}-acetic acid), and *p*-toluyglycylglycylsarcosine (Tol-GG-SAR, (methyl-{2-[2-(4-methyl-benzoylamino)-acetyl]amino}-acetyl)-amino)-acetic acid) were synthesized by dissolving known amounts of *p*-toluic acid (0.17–0.53 g) into sufficient volumes of dry DMF to dissolve in a vessel sealed to prevent exposure to water vapor. The synthesis procedures were the same as above for Tol-A, but 1.5 equiv of the appropriate amino acid/peptide were added via the following aqueous solutions: sarcosine, 5.2 M at pH 10.65; glycylsarcosine, 2.2 M at pH 10.0; and glycylglycylsarcosine, 1.3 M at pH 9.5. The reaction products were purified by preparative HPLC as described above. The collected fractions were dried in vacuo yielding clear, colorless films that were then dissolved in water. Tol-SAR crystallized as a white solid at  $5^\circ\text{C}$ . Tol-G-SAR and Tol-GG-SAR solutions were lyophilized yielding glassy solids. The proton NMR ( $^1\text{H}$  NMR) spectra of the sarcosine containing compounds were complicated by the presence of both *cis* and *trans* isomers of the *N*-methylated peptide bonds which caused splitting of many peaks into doublets of unequal size corresponding to the fractions of *cis* and *trans* present.  $^1\text{H}$  NMR ( $\text{D}_2\text{O}$ ) spectra are described as specifically as possible when the peaks are not overlapping. Tol-SAR:  $\delta$  7.2 (8-peaks, 4H, benzene ring), 4.02 (d, 2H,  $\text{CH}_2$ ), 2.97 (d, 3H,  $\text{N}-\text{CH}_3$ ), and 2.28 (d, 3H,  $-\text{CH}_3$ ); Tol-G-SAR:  $\delta$  7.62 (q, 2H, *o*), 7.27 (d, 2H, *m*), 4.14 (q, 4H, 2- $\text{CH}_2$ ), 2.98 (d, 3H,  $\text{N}-\text{CH}_3$ ), and 2.30 (s, 3H,  $-\text{CH}_3$ ); Tol-GG-SAR:  $\delta$  7.64 (d, 2H, *o*), 7.27 (d, 2H, *m*), 4.05 (6-peaks, 6H, 3- $\text{CH}_2$ ), 2.93 (d, 3H,  $\text{N}-\text{CH}_3$ ), and 2.30 (s, 3H,  $-\text{CH}_3$ ). The mass spectra were consistent with the indicated structures with parent ion peaks at  $m/z = 207$ , 264 and 321 for Tol-SAR, Tol-G-SAR and Tol-GG-SAR, respectively. Purity was >99% by HPLC for all three compounds.

*p*-Toluylsarcosylglycine (Tol-SAR-G, {2-[methyl-(4-methyl-benzoyl)-amino]-acetyl]amino}-acetic acid), *p*-Toluylsarcosyldiglycine (Tol-SAR-GG, (2-[2-[methyl-(4-methyl-benzoyl)-amino]-acetyl]amino)-acetyl]amino)-acetic acid), *p*-Toluyglycylsarcosyl-glycine (Tol-G-SAR-G, (2-{methyl-[2-(4-methyl-benzoylamino)-acetyl]-amino}-acetyl]amino)-acetic acid), and *p*-Toluyldisarcosylglycine (Tol-SAR-SAR-G, (2-(methyl-{2-[methyl-(4-methyl-benzoyl)-amino]-acetyl]-amino)-acetyl]amino)-acetic acid) were synthesized by the Department of Medicinal Chemistry, University of Utah, using a standard F-MOC solid-phase chemistry synthetic procedure and were then isolated by preparative scale HPLC as described above. The products were dried in vacuo yielding: a white solid for Tol-SAR-GG and clear, colorless films for Tol-SAR-G, Tol-G-SAR-G, and Tol-SAR-SAR-G, which were subsequently dissolved in water then lyophilized leaving glassy solids. The mass spectra were consistent with the indicated structures.  $^1\text{H}$  NMR ( $\text{D}_2\text{O}$ ) spectra are described as specifically as possible when the peaks are not overlapping. Tol-SAR-G:  $\delta$  7.3 (5-peaks (overlapped), 4H, benzene ring), 4.01 (q, 4H, 2- $\text{CH}_2$ ), 2.99 (d, 3H,  $\text{N}-\text{CH}_3$ ), and 2.28 (d, 3H,  $-\text{CH}_3$ ); Tol-SAR-GG:  $\delta$  7.3 (5-peaks (overlapped), 4H, benzene ring), 3.97 (5-peaks, 6H, 3- $\text{CH}_2$ ), 3.00 (s, 3H,  $\text{N}-\text{CH}_3$ ), and 2.28 (s, 3H,  $-\text{CH}_3$ ); Tol-G-SAR-G:  $\delta$  7.62 (t (overlapped), 2H, *o*), 7.27 (d, 2H, *m*), 4.09 (6-peaks, 6H,



3-CH<sub>2</sub>), 2.99 (d, 3H, N-CH<sub>3</sub>), and 2.30 (s, 3H, -CH<sub>3</sub>); Tol-SAR-SAR-G:  $\delta$  7.2 (11-peaks (overlapped), 4H, benzene ring), 4.07 (12-peaks, 6H, 3-CH<sub>2</sub>), 2.92 (8-peaks, 6H, 2-(N-CH<sub>3</sub>)), and 2.28 (d, 3H, -CH<sub>3</sub>). The mass spectra were consistent with the indicated structures with parent ion peaks at  $m/z$  = 264, 321, 321, and 335 for Tol-SAR-G, Tol-SAR-GG, Tol-G-SAR-G, and Tol-SAR-SAR-G, respectively. Purity was >99% by HPLC for all compounds.

(4-Methylcarbamoylmethyl-phenyl)-acetic acid and (4-dimethylcarbamoylmethyl-phenyl)-acetic acid were synthesized by dissolving 0.5 g 1,4-phenylenediacetic acid (PDAA) in 20 mL of dry DMF and cooling the resulting solution to <-10 °C in a dry ice/acetone bath. Diisopropylethylamine (1.2 equiv) was added into the solution followed by isobutyl chloroformate (1 equiv). The solution was stirred at <-10 °C for 10 min; then methylamine or dimethylamine (0.8 equiv) was added, and the reaction mixture was stirred at room temperature for 30 min. The product was purified by preparative HPLC and characterized by mass spectral analysis.

***pK<sub>a</sub> Measurements.*** The ionization constant for *p*-methylhippuric acid was reported earlier (12). The ionization constants for Tol-GG, Tol-GGG, Tol-SAR-G, Tol-SAR-GG, Tol-G-SAR-G, and Tol-SAR-SAR-G were determined at 25 °C using a microtitration technique (25) in which 150  $\mu$ L aliquots of 0.001–0.01 M solutions of each compound were titrated with NaOH. The *pK<sub>a</sub>* values of Tol-A, Tol-AA, Tol-AAA, Tol-SAR, Tol-G-SAR, and Tol-GG-SAR and the *p*-tolyl acetic acid series were each titrated using larger solution volumes, 1.0–3.6 mL, ranging in concentration from 0.004 to 0.032 M. Each sample was prepared in distilled/deionized water and stirred with water-saturated nitrogen gas during the titration with NaOH solution. Plots of pH versus volume of titrant were fitted to determine the thermodynamic *pK<sub>a</sub>* values (i.e., corrected for ionic strength) using the appropriate model.

The sarcosine-containing compounds were present as both trans and cis isomers, while unsubstituted peptides exist primarily in the trans configuration due to the differences in energy between the two states (26). *N*-Methylated amino acids, however, reduce the differences between these two states, allowing both isomers to exist. Evans and Rabenstein (24) showed that the two conformations create an environment different enough for the atoms surrounding the peptide bond that nearby ionizable groups may have different ionization constants in the two isomers. The cis isomer was found to be the more acidic of the two, suggesting that the protonated form of the trans isomer may be stabilized by intramolecular hydrogen bonding of the terminal carboxy with the carbonyl of the peptide bond, a conformation that is not possible in the cis configuration. In the present study, this effect appeared to be significant only when the *N*-methyl substituent is in the terminal position. The *pK<sub>a</sub>* values for these peptides measured by titration are macroscopic *pK<sub>a</sub>* values. Ionization constants for the individual conformers were derived from NMR spectra in D<sub>2</sub>O at two different pH values such that the spectra represented the completely ionized and un-ionized species of these weak acids according to the method of Evans and Rabenstein (24).

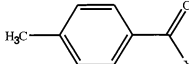
***Partition Coefficient Determinations.*** The 1,9-decadiene/water partition coefficient for *p*-methylhippuric acid was determined earlier (12), and the 1,9-decadiene/water partition

coefficients for Tol-A, Tol-AA, Tol-S, and Tol-G-SAR and for the *p*-tolyl acetic acid series were determined by the shake-flask method (27). Aliquots of aqueous solutions of peptide in 0.1 N HCl (*I* = 0.1 adjusted with NaCl) were added to volumes of 1,9-decadiene in triplicate. The partition coefficient for Tol-SAR was measured using three different starting concentrations to test for the possibility of concentration dependence, which was found to not be a factor. All samples were allowed to equilibrate for >24 h at 25 °C with occasional agitation. The phases were separated, and the compound in the 1,9-decadiene phase was collected and concentrated by extraction back to a fresh aqueous sample and analyzed by HPLC.

***Determination of Permeability Coefficients. LUV Preparation.*** The procedure employed to prepare LUVs was adapted from an earlier study (28). In short, accurately weighed quantities of egg-PC and egg-PA (for peptides) or DOPC/DOPA (*p*-tolyl acetic acid series) were dissolved in chloroform at a 96/4 (PC/PA) ratio. Aliquots of this solution were then transferred into 12  $\times$  75 mm culture tubes to provide 11.25 mg total lipid per tube. The chloroform was then removed under a dry nitrogen stream and the lipid samples were further dried in vacuo at ~50 °C for >30 min. An aqueous permeant solution (1.5 mL) in 0.04 M buffer, *I* = 0.1 (adjusted with NaCl) was added to the lipid film for a lipid concentration of 7.5 mg/mL. The aqueous solutions used the appropriate buffer species for each pH value (i.e., 2-(*N*-morpholino)ethanesulfonic acid (MES), phosphate, carbonate, tris(hydroxymethyl)amino-methane (Tris), and glycine). The lipids were suspended in the buffer solution by repeated vortexing at room temperature until the entire lipid film was removed from the glass surface. These lipid suspensions were then forced through 0.2  $\mu$ m polycarbonate filters (Nuclepore, Pleasanton, CA) 17 times each at room temperature to form the LUVs.

The average vesicle hydrodynamic diameter, *d*, in each vesicle solution was measured by dynamic light scattering (DLS). The DLS apparatus consisted of a goniometer/autocorrelator (Model BI-2030AT, Brookhaven, Holtsville, NY) and an Ar<sup>+</sup> ion laser (M95, Cooper Laser Sonics, Palo Alto, CA) operated at 514.5 nm wavelength. The solutions used in the DLS measurements were prepared by adding 1–2 drops of LUV solution to 2.0 mL of the respective buffer solution. The sample was then placed in a cuvette holder with a toluene index-matching bath at room temperature. Autocorrelation functions were determined for a period of 100 seconds with a 20  $\mu$ s duration at a 90° angle and analyzed by the method of cumulants.

***Transport Experiments.*** A 600  $\mu$ L aliquot of an LUV solution prepared as described above was loaded onto a size-exclusion column packed with Sephadex G-25M (PD-10 Sephadex G-25M, Supelco, Bellefonte, PA) in a 10 mL syringe which was thoroughly equilibrated with the same buffer (without permeant) that was used to prepare the LUV solution to ensure that the pH of the solutions inside and outside the LUVs was the same. The LUVs were then eluted by centrifugation (Model CL, IEC, Needham Hts., MA) at two successive speeds (2 min at 300g; 1 min at 500g). The void volume of the size exclusion column contained the vesicles with entrapped permeant sufficiently separated from free permeant in solution. The LUV solution was collected into a 12 mL glass vial that was capped and placed

Table 1: Structures and Physicochemical Properties of Peptides, Including the Number of Hydrogen Bonding Groups, Nonpolar Surface Areas of Amino Acid Side Chain Residues,  $pK_a$  Values, Intrinsic Permeabilities  $P_{HA}$ , 1,9-Decadiene/Water Partition Coefficients, and Functional Group Contributions


-X	$\Delta A_{np}^a$ (Å <sup>2</sup> )	no. of H-bonds	$pK_a^b$	$P_{HA} \pm S.D.$ (cm/s)	1,9-decadiene/ water PC $\pm$ SD	$\Delta(\Delta G^\circ)_X$ (kcal/mol)	
						from $P_{HA}$	from PC
-OH	0	2	4.36	$1.1 \pm 0.2^c$	$0.9 \pm 0.01^c$	0	0
-GLY	43.3	4	3.85	$(6.4 \pm 0.5) \times 10^{-4}$	$(3.4 \pm 1.2)^d \times 10^{-4}$	4.4	4.7
-GLY-GLY	86.6	6	3.87	$(4.2 \pm 0.5) \times 10^{-7}$	ND	8.7	ND
-GLY-GLY-GLY	129.9	8	3.93	$(1.7 \pm 0.3) \times 10^{-9}$	ND	12.0	ND
-ALA	80	4	3.83	$(2.3 \pm 0.2) \times 10^{-3}$	$(2.2 \pm 0.1) \times 10^{-3}$	3.7	3.6
-ALA-ALA	160	6	3.94	$(1.1 \pm 0.1) \times 10^{-5}$	$(1.1 \pm 0.3) \times 10^{-5}$	6.8	6.7
-ALA-ALA-ALA	240	8	3.99	$(9.5 \pm 0.8) \times 10^{-8}$	ND	9.6	ND
-SAR	43.3	3	3.37 (3.60, 3.15)	$(1.5 \pm 0.1) \times 10^{-3}$	$(1.0 \pm 0.2) \times 10^{-3}$	3.9	4.0
-SAR-GLY	86.6	5	3.65	$(3.2 \pm 0.3) \times 10^{-6}$	ND	7.5	ND
-GLY-SAR	86.6	5	3.42 (3.54, 3.18)	$(1.9 \pm 0.1) \times 10^{-5}$	$(1.6 \pm 0.3) \times 10^{-5}$	6.5	6.5
-SAR-GLY-GLY	129.9	7	3.59	$(1.4 \pm 0.1) \times 10^{-8}$	ND	10.8	ND
-GLY-SAR-GLY	129.9	7	3.62	$(4.8 \pm 0.4) \times 10^{-8}$	ND	10.0	ND
-GLY-GLY-SAR	129.9	7	3.40 (3.51, 3.14)	$(4.9 \pm 0.1) \times 10^{-8}$	ND	10.0	ND
-SAR-SAR-GLY	129.9	6	3.61	$(7.6 \pm 0.6) \times 10^{-8}$	ND	9.8	ND

<sup>a</sup> Solvent accessible surface areas for nonpolar amino acid side-chain residues from Wimley et al. (19). <sup>b</sup> Macroscopic  $pK_a$  values (from titration). Values in parentheses are microscopic  $pK_a$  values for trans and cis isomers, respectively, determined by NMR using the method of Evans and Rabenstein (24). <sup>c</sup> From Xiang et al. (13). <sup>d</sup> From Mayer (12).

immediately in a 25 °C water bath. After elution of the vesicles from the size-exclusion columns, there existed a permeant concentration gradient resulting in a net flux across the LUVs from inside to outside. To measure this flux the extravesicular permeant concentration was monitored at various time points. Aliquots (350  $\mu$ L) of the LUV solution after gel filtration were loaded onto Centricon-100 filters (MWCO = 100 000; Amicon, Beverly, MA). The loaded filter was then centrifuged at 1600g for 6–8 min. The Centricon-100 filters did not significantly affect permeant concentration when the filters were prerinsed with water and dried prior to use. Concentrations of the peptide permeants in the collected filtrates were analyzed by HPLC. The samples for HPLC analysis were analyzed without dilution except for the addition of a known quantity of concentrated hydrochloric acid to lower the pH of the solution to <3 for optimal compatibility with the mobile phase. The concentrations of *p*-methylhippuric acid at  $t_\infty$  (equilibrium) were measured by lysing a 350  $\mu$ L aliquot of the LUV solution after gel filtration with 8  $\mu$ L of Triton X-100 surfactant (Sigma, 10% in water) prior to HPLC analysis. For the other compounds of these peptide series, no special samples were prepared for  $t_\infty$ . Rather, the sampling times for the concentration versus time profiles were carried out to approximately 10 half-lives.

A modular HPLC system described previously (29) and a reversed-phase column packed with a 5  $\mu$ m, C-18, 300 Å stationary phase (Jupiter column 4.6 mm i.d.  $\times$  300 mm, Phenomenex, Torrance, CA) were used for all analyses. The mobile phase consisted of acetonitrile:water varying from 20% to 33% organic phase depending on the lipophilicity of the compound. The aqueous phase was buffered to a pH of 3.0 using 0.01 M ammonium phosphate.

The mathematical model used to fit the concentration versus time data of the transport experiments has been described in detail in an earlier publication (12). In short,

the concentration of permeant on the outside of the vesicles measured by HPLC,  $C_t$ , was fit versus time using eq 2:

$$C_t = C_\infty - (C_\infty - C_0)e^{(-k_{obs}t)} \quad (2)$$

In eq 2,  $k_{obs}$  is the first-order rate constant in  $h^{-1}$ , and  $C_\infty$  and  $C_0$  are the concentrations of permeant on the outside of the vesicle at equilibrium and  $t = 0$ , respectively. The transport data were fit to this equation by nonlinear least squares regression analysis using Scientist (Micromath Inc., Salt Lake City, UT) to solve for  $k_{obs}$ .

The apparent permeability coefficient,  $P_{app}$ , associated with each permeant at any pH can be obtained from this first-order rate constant and the ratio between the entrapped volume and surface area of the LUVs ( $P_{app} = k_{obs} * V_{in}/A$ ), where  $V_{in}/A$  is obtained from the vesicle hydrodynamic diameter,  $d$  ( $V_{in}/A = d/6$ ).

## RESULTS

**Physicochemical Properties of Peptides.** The structures of the peptides employed in these studies are shown in Table 1 along with *p*-toluic acid ( $X = -OH$ ) and *p*-methylhippuric acid ( $X = -GLY$ ). Solvent-accessible surface areas for the nonpolar portions of the peptide fragment side-chain residues,  $\Delta A_{np}$ , were based on values obtained by Wimley et al. (19) for AcGG-X-GG peptides. The number of potential hydrogen bonds that could be formed by each peptide were counted following a previously published procedure (30, 31). To calculate the fraction of un-ionized species,  $f_{HA}$ , present in each transport experiment at the various pH values, thermodynamic  $pK_a$  values were determined for each peptide at 25 °C. These  $pK_a$  values as well as that for *p*-toluic acid are also included in Table 1 along with the microscopic  $pK_a$  values for the trans and cis isomers of toluylsarcosine, toluylglycylsarcosine, and toluylglycylsarcosine determined

Table 2: Structures and  $pK_a$  Values, Intrinsic Permeabilities  $P_{HA}$ , 1,9-Decadiene/Water Partition Coefficients, and Functional Group Contributions for *p*-Tolylacetic Acid and  $\alpha$ -Methyl Substituted Analogs

-X	$pK_a$	$P_{HA} \pm S.D.$ (cm/s)	1,9-decadiene/ water PC $\pm$ SD	$\Delta(\Delta G^\circ)_X$ (cal/mol)	
				from $P_{HA}$	from PC
-H	4.40	$0.71 \pm 0.07$	0.40	0	0
-CONH(CH <sub>3</sub> )	4.25	$(3.4 \pm 0.3) \times 10^{-5}$	$2.6 \times 10^{-5}$	$5890 \pm 70$	5710
-CON(CH <sub>3</sub> ) <sub>2</sub>	4.33	$(3.3 \pm 0.2) \times 10^{-4}$	$(2.5 \pm 0.2) \times 10^{-4}$	$4540 \pm 70$	4370

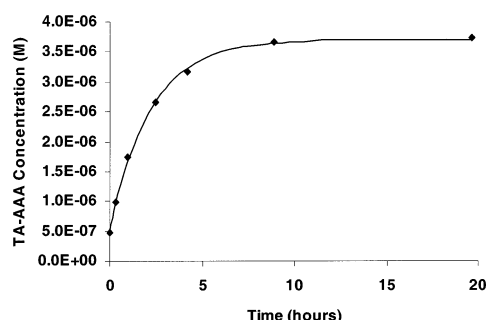
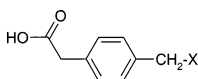
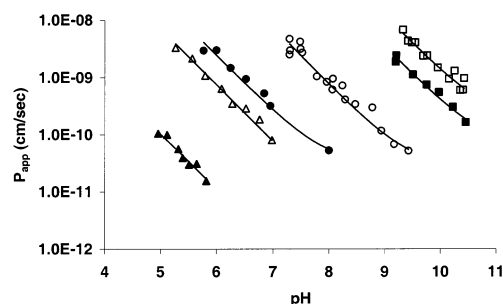
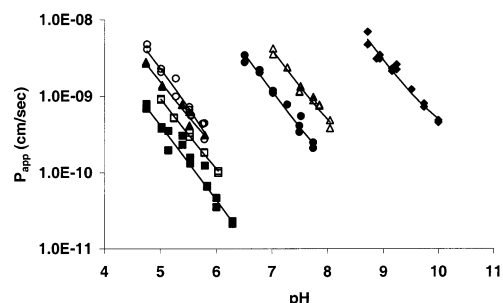


FIGURE 1: Concentration of Tol-AAA released from unilamellar vesicles vs time in suspensions at 25 °C and pH 6.28.

by NMR. Also included in Table 1 are the 1,9-decadiene/water partition coefficients of the compounds that could be measured by the shake-flask method described above. The partition coefficients of the more polar compounds could not be determined in this manner because of the extremely low concentrations present in the 1,9-decadiene phase. Table 2 contains additional data for the series of *p*-tolylacetic acids, including thermodynamic  $pK_a$  values at 25 °C and decadiene/water partition coefficients.

**Egg Lecithin Bilayer Permeability Coefficients.** Transport experiments were carried out using the egg lecithin LUV system at 25 °C for all peptides while DOPC/DOPA LUVs were used in determining permeability coefficients of the *p*-tolylacetic acids. Figure 1 shows a representative plot of  $C_t$  versus time for Tol-AAA at pH 6.28 along with the nonlinear least-squares fit of the data to eq 2. Such fits were used to generate first-order rate constants,  $k_{obs}$  associated with each compound at each pH. Apparent permeability coefficients,  $P_{app}$ , were calculated from the  $k_{obs}$  values using the average diameters (from DLS measurements) of the LUVs of each individual experiment as described above. The size of the LUVs ranged from 156 to 202 nm in diameter. The characterization and stability of the LUV systems over the wide range of pH values used in these studies has been reported earlier (32–34). The permeability coefficients of polar nonelectrolytes such as acetamide and D-mannitol across egg lecithin bilayers have been shown to be independent of solution pH (32, 34).

The pH ranges selected for transport experiments were chosen such that the transport was membrane-controlled rather than aqueous diffusion-controlled. At a given pH, the apparent permeability coefficient of a weak acid permeant can be expressed in terms of the relative contributions of the un-ionized ( $P_{HA}$ ) and ionized ( $P_{A-}$ ) species to the overall value as described in eq 3 where the fraction of un-ionized ( $f_{HA} = H^+/(H^+ + K_a/\gamma)$ ) and ionized ( $f_{A-} = 1 - f_{HA}$ ) species

FIGURE 2:  $\log P_{app}$  vs pH for all non-*N*-methylated peptides (toluyl-X). Legend: ■, X = -GLY; ●, X = -GLY-GLY; ▲, X = -GLY-GLY-GLY; □, X = -ALA; ○, X = -ALA-ALA; △, X = -ALA-ALA-ALA.FIGURE 3:  $\log P_{app}$  vs pH for all *N*-methylated peptides (toluyl-X). Legend: ◆, X = -SAR; △, X = -GLY-SAR; ▲, X = -GLY-SAR-GLY; ○, X = -SAR-SAR-GLY; ●, X = -SAR-GLY; ■, X = -SAR-GLY-GLY; □, X = -GLY-GLY-SAR.

are determined by the pH and the ionization constant ( $K_a/\gamma$ ) adjusted for an ionic strength of 0.1 using the Guntelberg approximation (35):

$$P_{app} = f_{HA} * P_{HA} + (1 - f_{HA}) * P_{A-} \quad (3)$$

Plots of  $\log(P_{app})$  versus pH are shown in Figures 2 (glycine and alanine series) and 3 (sarcosine-containing compounds) along with the nonlinear least-squares fits using eq 3. The slopes of  $-1.0$  with only slight curvature at the lower end of the permeability range indicate that the neutral species of each peptide, the concentration of which decreases 10-fold per unit increase in pH, accounts for the transport over the pH range explored. The intrinsic permeability coefficients for the un-ionized peptide species determined by nonlinear least squares regression analyses are shown in Table 1 along with the intrinsic permeability coefficient for *p*-toluic acid determined in an earlier study (32). Intrinsic permeability coefficients for the un-ionized *p*-tolylacetic acids across DOPC/DOPA bilayers determined by nonlinear least squares regression analyses are shown in Table 2.



## DISCUSSION

**Barrier Domain for Peptide Transport.** In contrast to early descriptions of membrane transport that assumed a membrane could be approximated by a homogeneous layer of bulk solvent into which a given permeant dissolved and diffused (36, 37), more accurate depictions recognize the inhomogeneous and anisotropic nature of lipid bilayer membranes. The influence of membrane heterogeneity on the permeability coefficient,  $P_m$ , of a compound at absolute temperature  $T$  can be described (38, 39) in terms of the depth dependence of the excess chemical potential and diffusion coefficient of the permeant in the membrane,  $\mu_{\text{exc}}(z)$  and  $D(z)$ , as shown by eq 4, where  $k_B$  is the Boltzmann constant and  $z$  is the depth:

$$P_m = 1/\int_{z_1}^{z_2} \frac{\exp[(\Delta\mu_{\text{exc}}(z) - \Delta\mu_{\text{exc}}^w)/k_B T]}{D(z)} dz \quad (4)$$

Recent statistical mechanical calculations (40) and molecular dynamics simulations of the permeation of small molecules across lipid bilayer membranes also indicate the need for an inhomogeneous solubility-diffusion model to describe both the position dependent diffusion and partitioning of small molecules (41–46). Experimentally, the inhomogeneous solubility-diffusion model is consistent with the preferential location of hexane within the relatively disordered bilayer center at equilibrium (47), while small peptides such as those employed in this study are located preferentially at the bilayer–water interface at equilibrium. For example, Jacobs and White (7, 48, 49) and later Brown and Huestis (50) demonstrated that the tripeptides Ala-X-Ala-O-*tert*-butyl (where X = –GLY, ALA, LEU, PHE, or TRP) are confined primarily to the interfacial region with nonpolar residues partially inserted into the hydrocarbon region. Equilibrium partitioning studies of peptide binding to bilayers (7, 8, 19) thus probe the bilayer interface rather than the hydrocarbon core region. Of interest in this study are the free energies of transfer of peptides into the hydrocarbon core region—information that cannot be readily obtained from equilibrium partitioning studies.

While the inhomogeneous solubility-diffusion model provides a more accurate depiction of the diffusion and concentration gradients observed both experimentally and computationally within lipid bilayer membranes, there is general agreement that among the various regions the dense, more ordered hydrocarbon chain region of the membrane poses the greatest resistance to transport of polar molecules such as the peptides of interest in this study and thus serves as the barrier domain for these molecules (12–14, 45, 51, 52). Integrating only over the relatively homogeneous barrier domain, eq 4 can be simplified to eq 5:

$$P_m = \frac{PC_{\text{bd/w}}D_{\text{bd}}}{d_{\text{bd}}} \quad (5)$$

where  $PC_{\text{bd/w}}$  is the barrier domain/water partition coefficient,  $D_{\text{bd}}$  is the diffusion coefficient of the permeant in the barrier domain, and  $d_{\text{bd}}$  is the thickness of this region. Thus, the assumption that the rates of transport of peptides across bilayers are governed by the dense hydrocarbon region of the bilayer provides a model consistent with the known

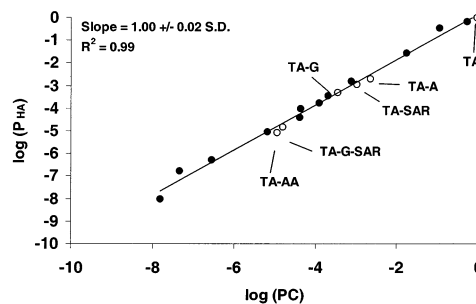


FIGURE 4: Linear correlation of the logarithms of intrinsic permeability coefficients across egg lecithin bilayers with logarithms of 1,9-decadiene/water partition coefficients for various substituted *p*-toluic and *p*-methylhippuric acids (filled symbols) and peptides from the present study (open symbols).

bilayer heterogeneity while retaining the simplicity of the homogeneous solubility-diffusion theory.

Experimental support for eq 5 is provided in Figure 4, where the logarithms of the egg lecithin bilayer permeability coefficients for a subset of the peptides listed in Table 1 are plotted versus the logarithms of their 1,9-decadiene/water partition coefficients (open symbols). (Peptides that were excluded from Figure 4 were those for which we were unable to obtain decadiene/water partition coefficients.) These results are superimposed on data from previous work for various substituted *p*-toluic and *p*-methylhippuric acids (closed symbols) (13, 34, 53). Remarkably, these permeability data spanning a range of approximately 8 orders-of-magnitude can be described by a simple linear free energy relationship described in eq 6:

$$\log(P_{\text{HA}}) = s \cdot \log(PC_{\text{org/w}}) + i \quad (6)$$

The slope of the line in Figure 4 has a value of  $1.0 \pm 0.02$  (SD). This slope, referred to as the selectivity coefficient (54), is a measure of the relative chemical affinities of a series of solutes for the barrier domain of the bilayer in comparison to the bulk organic solvent chosen for the correlation. The excellent correlation and slope of 1.0 in this plot establishes the hydrocarbon interior as the barrier domain for peptide permeability for permeants varying by over 8 orders-of-magnitude in lipophilicity. Figure 4 further suggests that differences in permeability coefficients reflect primarily the energetics of partitioning rather than differential changes in diffusion coefficients in egg PC versus decadiene for the peptides in this series, as increases in size and conformational flexibility did not result in deviations from the line in Figure 4. Previous experiments in these laboratories to explore the size and shape dependence of permeabilities across lipid bilayers (14) as well as theoretical calculations of the size-dependence of relatively large solutes (55) have suggested an exponential dependence of permeability on the minimum cross-sectional surface areas of the permeant. Studies of diffusion coefficients for dissolved gases in bulk solvents (56, 57) and  $C_5$  hydrocarbons in polyisobutylene (58) have similarly revealed a dependence of the diffusion coefficient on cross-sectional surface areas. The peptides in this study have similar minimum cross sectional surface areas in their fully extended conformations (12).

**Hydrogen Bond Potential as a Predictor of Peptide Permeability.** The importance of the desolvation of hydrogen-bonding groups accompanying the transfer of peptides from

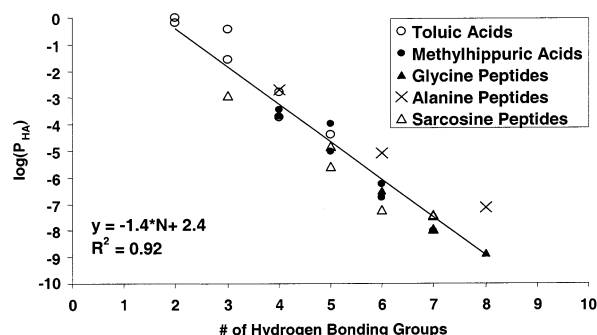


FIGURE 5: Plot of  $\log(P_{HA})$  vs the number of hydrogen bonding sites on each permeant.

water into the membrane interior is widely acknowledged (30). Roseman estimated the energetic cost of transferring a single peptide backbone  $-\text{CONH}-$  residue from water into  $\text{CCl}_4$  to be 6.1 kcal (10). This substantial penalty suggests that desolvation of hydrogen bonding groups may be a dominant force governing peptide permeability. Conradi et al. reached this conclusion in an examination of the Caco-2 cell permeabilities of a series of Phe-containing peptides up to the tetrapeptide, in which they demonstrated a linear relationship between the logarithm of monolayer permeability and the number of potential hydrogen-bonding sites in the solute (31, 59). They further argued that hydrogen-bonding number or an experimental measure of the hydrogen-bonding potential such as  $\Delta\log PC$ , the difference between the logarithms of the octanol/water and hydrocarbon/water partition coefficients, were superior to organic solvent/water partition coefficients for correlating their permeability data (60).

The number of hydrogen bonding sites for the peptides investigated in this study are listed in Table 1, calculated as described by Chikhale et al. (61). Shown in Figure 5 is the relationship between egg lecithin bilayer permeability and hydrogen-bond number for the peptides of this study plus the methyl-substituted *p*-toluic and *p*-methylhippuric acids for which the intrinsic permeability coefficients were published earlier (12, 13). Although the correlation in Figure 5 is quite good ( $r^2 = 0.92$ ), it is clear that the correlation with decadiene/water partition coefficients in Figure 4 is superior. Decadiene/water partitioning appears to capture not only the effects of hydrogen-bond desolvation but other forces that also play a significant, though perhaps not a dominant role, in the overall permeability. The slope of  $-1.4$  in the regression line in Figure 5 is significantly more negative than that ( $\sim -0.35$ ) reported by Conradi et al. in their studies of Caco-2 cell permeability (31). Evidently the egg lecithin bilayers exhibit substantially greater selectivity toward hydrogen-bonding groups than the Caco-2 membrane barrier.

**Residue Contributions to the Apparent Free Energies of Peptide Transfer.** A closer examination of the data in Figure 5 reveals that, for a given number of H-bonding sites, deviations of more than  $\pm 1$  order of magnitude are frequently observed, indicating that structural features in addition to the number of hydrogen-bonding sites must also be considered.

The contributions to the apparent free energies of transfer from water into the barrier domain,  $\Delta(\Delta G^\circ)_X$ , due to each amino acid residue were calculated using eq 1 versus toluic acid as the reference permeant.

The next level of complexity beyond assuming that transfer free energies reflect only hydrogen-bond desolvation is to assume that the polar and nonpolar portions of the peptides contribute additively to the overall solvation energies. Eisenberg et al. (1, 2) calculated the free energy difference between the folded state and unfolded state of proteins by expressing the standard free energy of transfer in terms of accessible surface areas ( $A_i$ ) of each atom  $i$  ( $\Delta G^\circ = \sum \Delta\sigma_i A_i$ ), where the  $\Delta\sigma_i$  values were derived from the octanol/water partition coefficients of acetyl amino acid amides measured by Fauchère and Pliška (3) and the accessible surface areas were calculated from the amino acid residues, X, in a Gly-X-Gly sequence in an extended conformation. Recent applications of this approach for neutral compounds have employed a simplified treatment in terms of only two solvation parameters reflecting the additive contributions of polar and nonpolar residues without regard to the specific nature of the substituents (19, 62).

We calculated solvation parameters for the peptides in Table 1 by fitting the transfer free energies to eq 7:

$$\Delta(\Delta G^\circ)_X = \text{const} + \sigma_{np}\Delta A_{np} + n_{-\text{CONH}-}\Delta\Delta G_{-\text{CONH}-} + n_{\text{Tol}-\text{CONMe}-}\Delta\Delta G_{\text{Tol}-\text{CONMe}-} + n_{-\text{CONMe}-}\Delta\Delta G_{-\text{CONMe}-} \quad (7)$$

where solvent-accessible surface areas for the nonpolar portions of the peptide fragment side-chain residues,  $\Delta A_{np}$ , were taken from Wimley et al. for AcGG-X-GG peptides (19). We considered separately the peptide bonds ( $-\text{CONH}-$  and  $-\text{CON}(\text{Me})-$ ) and allowed the solvation parameters for *N*-methylated peptide bonds attached directly to toluic acid ( $\Delta\Delta G_{\text{Tol}-\text{CONMe}-}$ ) to differ from those elsewhere in the peptide.

$\Delta(\Delta G^\circ)_X$  values calculated from the above equation are compared to the experimental values in Figure 6. The solvation parameters obtained from this regression analysis are listed in Table 3 and compared to literature values for peptide partitioning into octanol or interfacial binding to the bilayer. The coefficient of determination for this regression analysis was 0.9928. Inclusion of a constant term ( $\text{const} = 926 \pm 245 \text{ cal/mol}$ ) significantly improved the fit of the data. This constant term may be necessary to account for the change in solvation energy when the terminal carboxylic acid residue is an aliphatic rather than an aromatic substituent.

**Nonpolar Residue Solvation Parameter.** Several groups have estimated the nonpolar residue solvation parameter, typically expressed as a positive quantity to represent solute transfer from organic solvent to water. The results reported in Table 3 refer to the transfer of permeant from water to the organic phase and are therefore negative quantities for nonpolar residues. Reynolds et al. (63) estimated a value of  $-21$  to  $-25 \text{ cal/mol/\AA}^2$  from hydrocarbon solubility data; Chothia (64) obtained a value of  $-22 \text{ cal/mol/\AA}^2$  from transfer free energies of amino acids from water to organic solvent generated by Nozaki and Tanford (65), while Rose et al. (66) obtained  $-18.9 \text{ cal/mol/\AA}^2$  from the same data set. More recently, Wimley et al. (8, 19) have generated the results shown in Table 3 for octanol/water partitioning of peptides ( $-22.8$  and  $-20.9 \text{ cal/mol/\AA}^2$ ) and  $-13.9$  for interfacial binding to phospholipid bilayers. Our result for  $\sigma_{np}$  ( $-20.8 \text{ cal/mol/\AA}^2$ ) representing the transfer of permeant from water to the dense hydrocarbon chain region of egg





Table 5: Effect of *N*-Methylation on the Incremental Free Energies of Transfer from Water into the Egg Lecithin Bilayer Barrier Domain,  $\Delta(\Delta G^\circ)_X$ , Obtained by Comparing Sarcosine-Containing Peptides with Their Glycine-Containing Counterparts

entry line	reference compound	substituted compound	substituent alteration	$\Delta(\Delta G^\circ)_X \pm \text{S.D.}$ (cal/mol)
1	Tol-G	Tol-SAR	N-H $\rightarrow$ N-CH <sub>3</sub>	-503 $\pm$ 67
2	Tol-G-G	Tol-SAR-G	N-H $\rightarrow$ N-CH <sub>3</sub>	-1240 $\pm$ 80
3	Tol-G-G-G	Tol-SAR-G-G	N-H $\rightarrow$ N-CH <sub>3</sub>	-1230 $\pm$ 100
4	Tol-G-SAR-G	Tol-SAR-SAR-G	N-H $\rightarrow$ N-CH <sub>3</sub>	-288 $\pm$ 70
5	Tol-G-G	Tol-G-SAR	N-H $\rightarrow$ N-CH <sub>3</sub>	-2220 $\pm$ 70
6	Tol-G-G-G	Tol-G-SAR-G	N-H $\rightarrow$ N-CH <sub>3</sub>	-1950 $\pm$ 80
7	Tol-G-G-G	Tol-G-G-SAR	N-H $\rightarrow$ N-CH <sub>3</sub>	-1970 $\pm$ 60
8	Tol-SAR-G-G	Tol-SAR-SAR-G	N-H $\rightarrow$ N-CH <sub>3</sub>	-1010 $\pm$ 80
9	Tol-A	Tol-SAR	C-CH <sub>3</sub> $\rightarrow$ N-CH <sub>3</sub>	310 $\pm$ 80

lipid bilayer. Both the nonadditivity and the reduced incremental free energy contribution for the  $-\text{CONH}-$  in a peptide backbone compared to its "isolated" contribution may be rationalized by considering the possible role of conformational effects and the increased intramolecular hydrogen bonding accompanying the transfer of a peptide from water to a nonpolar environment. We first consider the possible role of the seven-membered ring formed by  $3 \rightarrow 1$  intramolecular hydrogen bonding between the carboxylic acid terminus and the carbonyl group adjacent to the C terminus (the  $C_7$  conformer).

Madison and Kopple (20) analyzed the conformational distributions of AcProNHMe and AcAlaNHMe using circular dichroism,  $^{13}\text{C}$  chemical shifts, and  $^1\text{H}$  nuclear Overhauser experiments to confirm conclusions from infrared analyses of N-H stretching in dilute  $\text{CCl}_4$  solution that the intramolecularly hydrogen bonded  $C_7$  conformations predominate in nonpolar solvents (e.g., AcAlaNHMe exists about 70% in the  $C_7$  form in  $\text{CCl}_4$ ) while in water the  $C_7$  conformer is probably absent. Madison and Delaney (70) demonstrated that the *syn*- and *anti*-Ac-3-Me-ProNHMe differ significantly in fraction of  $C_7$  conformer, with the anti isomer 90%  $C_7$  in  $\text{CCl}_4$  while the *syn* isomer is only 60%  $C_7$ . The free energies of transfer from carbon tetrachloride to water were  $-4.1$  kcal/mol for the anti isomer and  $-4.7$  kcal/mol for *syn*-Ac-3-Me-ProNHMe, which they concluded were attributable to differences in the population of the intramolecularly hydrogen-bonded  $C_7$  conformer. Evidence for  $C_7$  conformers involving a  $-\text{COOH}$  terminus also exists. Toniolo et al. (71) examined the temperature dependence of *cis*-*trans* isomerism of the  $-\text{CONH}-$  bond in the t-BOC derivatives of L-valine, L-alanine, and L-phenylalanine in deuteriochloroform using proton magnetic resonance and infrared absorption spectroscopy, concluding that the L-Ala and L-Phe exhibited a markedly higher population of the *trans* form than the L-Val derivative due to stabilization of the *trans* form by  $3 \rightarrow 1$  intramolecular hydrogen bonding to form a seven-membered ring. These observations suggest that the backbone  $-\text{CONH}-$  contribution obtained in Table 3, even that for the smallest peptides in our study (e.g., Tol-A and Tol-G), reflects the contribution of intramolecularly hydrogen-bonded states. Increasing peptide length allows the formation of more stable intramolecularly hydrogen-bonded conformations. Model dipeptides having the sequence t-BOC-L-Pro-Xaa-NHMe (Xaa = L- or D-Leu, Val, Cys, Met, Phe, and Tyr), the smallest molecules capable of forming  $\beta$ -folded conformers through formation of a 10-membered ring involving an  $i + 3 \rightarrow i$  intramolecular hydrogen bond, have been shown to exist predominantly in  $\beta$ -folded conformations in  $\text{CHCl}_3$  by

both  $^1\text{H}$  NMR and IR spectroscopy (72). Infrared spectra for Ac-Pro-Leu-Gly-NH<sub>2</sub> and trifluoroacetyl-Pro-Leu-Gly-NH<sub>2</sub> in chloroform have been interpreted in terms of an equilibrium between a hydrogen-bond free conformer and two hydrogen-bonded conformers with 10- and 13-membered rings corresponding to the  $\beta$ -turn and  $\alpha$ -helix, respectively (21, 22). Decreases in  $\Delta(\Delta G^\circ)_X$  for the Gly and Ala contributions noted in Table 4 may reflect the likely participation of  $-\text{CONH}-$  residues in increasingly favorable intramolecularly hydrogen-bonded conformers with increasing peptide length.

*Nonadditivity in  $\Delta(\Delta G^\circ)_X$  for N-Methylation.* The results of the regression analysis shown in Table 3 suggest that a single *N*-methylation of a normal (i.e., aliphatic) peptide bond reduces the peptide bond ( $-\text{CONH}-$ ) contribution by approximately 1.7 kcal/mol, resulting in a  $\sim 20$ -fold more favorable permeability coefficient. As a point of reference, the incremental contribution of a second *N*-methyl on a completely isolated  $-\text{CONHCH}_3$  substituent at the *para*-methyl position of *p*-tolylacetic acid is  $\sim 1340$ – $1350$  cal/mol when calculated either from bilayer permeability coefficients or 1,9-decadiene/water partition coefficients (Table 2), significantly smaller than that found for the average *N*-methyl contribution within the peptides explored in this study. The impact of *N*-methylation appears to be substantially reduced (less favorable) when the *N*-methylation occurs at the toluamide nitrogen (i.e., the first amide bond), reducing the incremental free energy contribution of the peptide bond by only 0.7 kcal/mol, as determined by regression analysis (Table 3). These observations again challenge the notion of additivity implicit in attempts to obtain a single value for the contribution of a peptide bond to the transfer free energy.

More dramatic evidence of nonadditivity can be found in the position dependence of  $\Delta(\Delta G^\circ)_X$  for *N*-methyl substitution obtained by examining the sarcosine-containing peptides shown in Table 5. While the  $\Delta(\Delta G^\circ)_X$  values are all negative, indicating that the replacement of N-H with N-CH<sub>3</sub> increases the rate of transport in all cases, the range of increase in flux varies from  $\sim 1.6$ - to 42-fold. In each of these comparisons, the compounds vary only slightly and by the same increment in molecular weight so differences in the apparent free energy contributions are not due to molecular volume effects, though shape effects cannot be ruled out.

Interpretation of the effects of *N*-methylation are complicated by the fact that whereas secondary amides exist only in the *trans* configuration (26), *N*-methylation results in a significant population of the *cis* isomer apparently induced by a bulky substituent on the amide nitrogen (24, 73). Since the rate of rotation about the  $-\text{C}-\text{N}$  peptide bonds is slow

on the NMR time scale, the fraction of peptide bonds present as cis isomers can be obtained from the cis/trans peak ratios detected by  $^1\text{H}$  NMR measurements (24). At high pD values (pD = 9.1–11.1), the percentage of cis isomer for the compounds in Table 1 was found to range from a low value of 29% for Tol-G-SAR-G to a high of 65% for Tol-SAR. In all of the peptides then, there are significant fractions of the molecules existing as the cis isomers. Due to the positions of atoms around the peptide bond, the intramolecular hydrogen-bonded  $\text{C}_7$  conformer can exist only in the trans isomer. Yet, despite the fact that intramolecular hydrogen-bonding is precluded for the cis fraction, several lines of evidence support the existence of  $\text{C}_7$  conformers in N-alkylated peptides. Variable-temperature infrared studies in relatively nonpolar organic solvents (e.g.,  $\text{CCl}_4$ ) show significant populations of the internally hydrogen-bonded species of acetyl-*N*-methyl-DL-norleucine *N*-methanamide and acetylsarcosine *N*-methanamide (74). Gerig (75) suggested that intramolecular hydrogen-bonding leads to a predominance of the trans isomer of the  $-\text{COOH}$  forms of acetyl sarcosine and Gly-Sar and may be sufficiently strong to compete with water molecules in aqueous solutions. As demonstrated in Table 1, different microscopic  $\text{pK}_a$  values were evident for the cis and trans isomers of compounds containing a sarcosine terminus from the pH dependence of the cis/trans peak ratios. The higher  $\text{pK}_a$  for the trans isomer has been taken as evidence for intramolecular hydrogen bonding in the trans isomer (24).

The presence of cis isomers and the accompanying disruption of  $\text{C}_7$  conformers that are likely to promote partitioning into the bilayer interior (due to nonpolar solvent induced folding) may account for the substantially more positive than expected  $\Delta(\Delta G^\circ)_X$  ( $-0.5$  kcal/mol) for the conversion of Tol-G to Tol-Sar. The surprising nature of this result can be further appreciated by comparing the effect of an additional  $-\text{CH}_3$  substituent in Tol-G  $\rightarrow$  Tol-A with that in Tol-G  $\rightarrow$  Tol-SAR (Table 3). Relocation of the methyl group from the  $\alpha$ -methylene of Tol-A to the amide nitrogen in Tol-SAR results in an incremental change in its contribution of  $+310$  cal/mol, indicating that despite the loss of a polar hydrogen bond donating group on *N*-methylation in the case of Tol-SAR, its rate of transport is actually slower than that of Tol-A. This supports the viewpoint that the relatively less favorable  $\Delta(\Delta G^\circ)_X$  for *N*-methylation to form Tol-Sar may be rationalized by disruption of intramolecular hydrogen bonding accompanying the shift from predominantly trans isomers to a mixture of cis and trans configurations.

In general, methylation of the first peptide bond in the series examined yields more positive values of  $\Delta(\Delta G^\circ)_X$  than the "reference" value of  $\sim -1.3$  kcal/mol, possibly due to constraints on the types of intramolecularly hydrogen-bonded species that can form when the first peptide bond exists partially in cis form. Additional studies will be necessary, however, to rule out the possibility that the less favorable effect of *N*-methylation at the first peptide bond is not unique to the toluamide-containing peptides. *N*-Methylation of Tol-G-SAR-G to form Tol-SAR-SAR-G, results in the least favorable  $\Delta(\Delta G^\circ)_X$  of only  $-288$  cal/mol, suggesting that successive *N*-methylations may have a diminishing influence on promoting permeability or membrane insertion.

The apparent contributions for *N*-methylation beyond the first peptide bond are generally greater than the "reference"  $\Delta(\Delta G^\circ)_X$  for *N*-methylation. While it is tempting to speculate that intramolecular hydrogen bonding may be promoted by *N*-methylation in these cases, we are not aware of any experimental evidence pertaining to this question.

## SUMMARY

We have demonstrated that functional group effects on peptide transport across lipid bilayer membranes can provide useful information pertaining to the free energies of peptide transfer from water into the hydrocarbon chain interior of lipid membranes (i.e., the barrier domain). Whereas the solvation parameter derived from the atomic solvent-accessible surface areas of nonpolar amino acid residues (this study) resembles those obtained from peptide partitioning from water to the bilayer interface or from octanol/water partition coefficients, our result for the apparent incremental free energy contribution for the transfer of the peptide bond ( $-\text{CONH}-$ ) from water to the barrier domain (4.6 kcal/mol) reveals that the barrier domain is substantially more nonpolar than the region probed in peptide bilayer/water partition coefficient measurements. The present method may have greater utility in estimating thermodynamic quantities for peptide/protein insertion into the hydrocarbon core of membranes.

The value of  $\Delta(\Delta G^\circ)_{-\text{CONH}-}$  ( $= 4.6$  kcal/mol) for peptide bond transfer into the egg lecithin lipid bilayer barrier domain resembles that for peptide partitioning from water to 1,9-decadiene but is significantly less than the  $\Delta(\Delta G^\circ)_{-\text{CONH}-}$  ( $\sim 6.1$  kcal/mol) estimated for an isolated  $-\text{CONH}-$  in non-peptides. This reduced value for the peptide backbone  $-\text{CONH}-$ , nonadditivities observed in  $\Delta(\Delta G^\circ)_{-\text{CONH}-}$ , and dramatic variability in the effects of *N*-methylation depending on position within the peptide may reflect the influence of membrane induced or enhanced intramolecular hydrogen bonding to form folded conformations having more favorable free energies in the nonpolar hydrocarbon region of lipid bilayers. Simple predictive relationships based on the assumption of additivity and independence of peptide fragment contributions fail to accurately predict the thermodynamics of peptide partitioning into the hydrocarbon region of lipid membranes without a consideration of membrane induced changes in conformation and the distribution of various conformational states in the membrane and water. We are exploring these questions in further experimental studies and in molecular dynamics simulations of peptide conformation in membrane bilayers and in water.

## ACKNOWLEDGMENT

The authors wish to thank Dr. Robert Schackmann currently of the Huntsman Cancer Institute, Salt Lake City, UT, and Yichen Cao, University of Kentucky, for the synthesis of several of the compounds in this study.

## REFERENCES

1. Eisenberg, D., and McLachlan, A. D. (1986) Solvation energy in protein folding and binding. *Nature* 319, 199–203.
2. Eisenberg, D., Wesson, M., and Yamashita, M. (1989) Interpretation of protein folding and binding with atomic solvation parameters. *Chem. Scr.* 29A, 217–221.



3. Fauchere, J.-L., and Pliska, V. (1983) Hydrophobic parameters  $\pi$  of amino acid side chains from the partitioning of *N*-acetyl-amino acid amides, *Eur. J. Med. Chem. - Chim. Ther.* 18, 369–375.
4. Kim, A., and Szoka, J., F. C. (1992) Amino acid side-chain contributions to free energy of transfer of tripeptides from water to octanol, *Pharm. Res.* 9, 504–514.
5. Karplus, P. A. (1997) Hydrophobicity regained, *Protein Sci.* 6, 1302–1307.
6. Radzicka, A., and Wolfenden, R. (1988) Comparing the polarities of the amino acids: Side-chain distribution coefficients between the vapor phase, cyclohexane, 1-octanol, and neutral aqueous solution, *Biochemistry* 27, 1664–1670.
7. Jacobs, R. E., and White, S. H. (1989) The nature of the hydrophobic binding of small peptides at the bilayer interface: Implications for the insertion of transbilayer helices, *Biochemistry* 28, 3421–3437.
8. Wimley, W. C., and White, S. H. (1996) Experimentally determined hydrophobicity scale for proteins at membrane interfaces, *Nat. Struct. Biol.* 3, 842–848.
9. White, S. H., and Wimley, W. C. (1998) Hydrophobic interaction of peptides with membrane interfaces, *Biochim. Biophys. Acta* 1376, 339–352.
10. Roseman, M. A. (1988) Hydrophobicity of the peptide C=O---H-N hydrogen-bonded group, *J. Mol. Biol.* 201, 621–623.
11. Ben-Tal, N., Ben-Shaul, A., Nicholis, A., and Honig, B. (1996) Free-energy determinants of  $\alpha$ -helix insertion into lipid bilayers, *Biophys. J.* 70, 1803–1812.
12. Mayer, P. T. (2001) *Department of Pharmaceutics & Pharmaceutical Chemistry*, Ph.D. Thesis, pp 227, University of Utah, Salt Lake City.
13. Xiang, T.-X., and Anderson, B. D. (1994) Substituent contributions to the permeability of substituted *p*-toluic acids in lipid bilayer membranes, *J. Pharm. Sci.* 83, 1511–1518.
14. Xiang, T.-X., and Anderson, B. D. (1998) Influence of chain ordering on the selectivity of dipalmitoylphosphatidylcholine bilayer membranes for permeant size and shape, *Biophys. J.* 75, 2658–2671.
15. Thorgeirsson, T. E., Russell, C. J., King, D. S., and Shin, Y.-K. (1996) Direct determination of the membrane affinities of individual amino acids, *Biochemistry* 35, 1803–1809.
16. Ladokhin, A. S., and White, S. H. (1999) Folding of amphipathic  $\alpha$ -helices on membranes: Energetics of helix formation by melittin, *J. Mol. Biol.* 285, 1363–1369.
17. Hunt, J. F., Earnest, T. N., Bousche, O., Kalghatgi, K., Reilly, K., Horvath, C., Rothschild, K. J., and Engelman, D. M. (1997) A biophysical study of integral membrane protein folding, *Biochemistry* 36, 15156–15176.
18. Hunt, J. F., Rath, P., Rothschild, K. J., and Engelman, D. M. (1997) Spontaneous, pH-dependent membrane insertion of a trans-bilayer  $\alpha$ -helix, *Biochemistry* 36, 15177–15192.
19. Wimley, W. C., Creamer, T. P., and White, S. H. (1996) Solvation energies of amino acid side chains and backbone in a family of host-guest pentapeptides, *Biochemistry* 35, 5109–5124.
20. Madison, V., and Dopple, K. D. (1980) Solvent-dependent conformational distributions of some dipeptides, *J. Am. Chem. Soc.* 102, 4855–4863.
21. Tonan, K., and Ikawa, S. (1997) High-pressure FTIR study of intramolecular hydrogen bonding and conformation of a small peptide in solution, *Spectrochim. Acta A* 53, 2695–2700.
22. Tonan, K., and Ikawa, S. (1996) Intramolecular hydrogen bonding and conformation of small peptides: Variable-temperature FTIR study on *N*-acetyl-L-pro-L-leu-gly-NH<sub>2</sub> and related compounds, *J. Am. Chem. Soc.* 118, 6960–6965.
23. Gray, R. A., Vander Velde, D. G., Burke, C. J., Manning, M. C., Middaugh, C. R., and Borchardt, R. T. (1994) Delta-sleep-inducing peptide: Solution conformational studies of a membrane-permeable peptide, *Biochemistry* 33, 1323–1331.
24. Evans, C. A., and Rabenstein, D. L. (1974) Nuclear magnetic resonance studies of the acid-base chemistry of amino acids and peptides. II. Dependence of the acidity of the C-terminal carboxyl group on the conformation of the C-terminal peptide bond, *J. Am. Chem. Soc.* 96, 7312–17.
25. Morgan, M. E., Liu, K., and Anderson, B. D. (1998) Microscale titrimetric and spectrophotometric methods for determination of ionization constants and partition coefficients of new drug candidates, *J. Pharm. Sci.* 87, 238–245.
26. Marsh, R. E., and Donohue, J. (1967) Crystal structure studies of amino acids and peptides, *Adv. Protein Chem.* 22, 235–256.
27. Leo, A., Hansch, C., and Elkins, D. (1971) Partition coefficients and their uses, *Chem. Rev.* 71, 525–616.
28. Xiang, T.-X., Xu, Y.-H., and Anderson, B. D. (1998) The barrier domain for solute permeation varies with lipid bilayer phase structure, *J. Membr. Biol.* 165, 77–90.
29. Xiang, T.-X., and Anderson, B. D. (2000) Influence of a transmembrane protein on the permeability of small molecules across lipid membranes, *J. Membr. Biol.* 173, 187–201.
30. Stein, W. D. (1967) in *The Movement of Molecules Across Cell Membranes*, pp 65–125, Academic Press, New York.
31. Conradi, R. A., Hilgers, A. R., Ho, N. F. H., and Burton, P. S. (1991) The influence of peptide structure on transport across Caco-2 cells, *Pharm. Res.* 8, 1453–1459.
32. Xiang, T.-X., Chen, X., and Anderson, B. D. (1992) Transport methods for probing the barrier domain of lipid bilayer membranes, *Biophys. J.* 63, 78–88.
33. Xiang, T.-X., and Anderson, B. D. (1995) Development of a combined NMR paramagnetic ion-induced line-broadening/dynamic light scattering method for permeability measurements across lipid bilayer membranes, *J. Pharm. Sci.* 84, 1308–1315.
34. Mayer, P., Xiang, T.-X., and Anderson, B. D. (2000) Independence of substituent contributions to the transport of small molecule permeants in lipid bilayers, *AAPS PharmSci* 2 (2), 1–13 (<http://www.pharmsci.org/>).
35. Butler, J. N. (1998) *Ionic Equilibrium. Solubility and pH Calculations*, John Wiley & Sons, Inc., New York.
36. Overton, E. (1899) Ueber die allgemeinen osmotischen Eigenschaften der Zelle, ihre vermutlichen Ursachen und ihre Bedeutung für die Physiologie, *Vjschr. Naturforsch. Ges. Zurich* 44, 88.
37. Finkelstein, A. (1976) Water and nonelectrolyte permeability of lipid bilayer membranes., *J. Gen. Physiol.* 68, 127–135.
38. Diamond, J. M., Szabo, G., and Katz, Y. (1974) Theory of nonelectrolyte permeation in a generalized membrane, *J. Membr. Biol.* 17, 148–152.
39. Pohorille, A., Wilson, M. A., Chipot, C., New, M. H., and Schweighofer, K. (1999) in *Computational Molecular Biology* (Leszczynski, J., Ed.) pp 485–535, Elsevier Science B.V., New York.
40. Xiang, T.-X., and Anderson, B. D. (1994) Molecular distributions in lipid bilayers and other interphases: A statistical mechanical theory combined with molecular dynamics simulation, *Biophys. J.* 66, 561–573.
41. Bassolino-Klimas, D., Alper, H. E., and Stouch, T. R. (1993) Solute diffusion in lipid bilayer membranes: An atomic level study by molecular dynamics simulation, *Biochemistry* 32, 12624–12637.
42. Bassolino-Klimas, D., Alper, H. E., and Stouch, T. R. (1995) Mechanism of solute diffusion through lipid bilayer membranes by molecular dynamics simulation, *J. Am. Chem. Soc.* 117, 4118–4129.
43. Alper, H. E., and Stouch, T. R. (1995) Orientation and diffusion of a drug analogue in biomembranes: molecular dynamics simulations, *J. Phys. Chem.* 99, 5724–5731.
44. Marrink, S. J., and Berendsen, H. J. C. (1994) Simulation of water transport through a lipid membrane, *J. Phys. Chem.* 98, 4155–4168.
45. Marrink, S. J., and Berendsen, H. J. C. (1996) Permeation process of small molecules across lipid membranes studied by molecular dynamics simulations, *J. Phys. Chem.* 100, 16729–16738.
46. Xiang, T.-X. (1999) Translational diffusion in lipid bilayers: Dynamic free-volume theory and molecular dynamics simulation, *J. Phys. Chem. B* 103, 385–394.
47. White, S. H., King, G. I., and Cain, J. E. (1981) Location of hexane in lipid bilayers determined by neutron diffraction, *Nature* 290, 161–163.
48. Jacobs, R. E., and White, S. H. (1986) Mixtures of a series of homologous hydrophobic peptides with lipid bilayers: A simple model system for examining the protein-lipid interface, *Biochemistry* 25, 2605–2611.
49. Jacobs, R. E., and White, S. H. (1987) Lipid bilayer perturbations induced by simple hydrophobic peptides, *Biochemistry* 26, 6127–6134.
50. Brown, J. W., and Huestis, W. H. (1993) Structure and orientation of a bilayer-bound model tripeptide. A <sup>1</sup>H NMR study, *J. Phys. Chem.* 97, 2967–2973.
51. Xiang, T.-X., and Anderson, B. D. (2002) A computer simulation of functional group contributions to free energy in water and a DPPC lipid bilayer, *Biophys. J.* 82, 2052–2066.
52. Xiang, T.-X., and Anderson, B. D. (1997) Permeability of acetic acid across gel and liquid-crystalline lipid bilayers conforms to free-surface-area theory, *Biophys. J.* 72, 223–237.

53. Mayer, P. T., and Anderson, B. D. (2002) Transport across 1,9-decadiene precisely mimics the chemical selectivity of the barrier domain in egg lecithin bilayers, *J. Pharm. Sci.* **91**, 640–646.
54. Diamond, J. M., and Katz, Y. (1974) Interpretation of nonelectrolyte partition coefficients between dimyristoyl lecithin and water, *J. Membr. Biol.* **17**, 121–154.
55. Mitragotri, S., Johnson, M. E., Blankschtein, D., and Langer, R. (1999) An analysis of the size selectivity of solute partitioning, diffusion, and permeation across lipid bilayers, *Biophys. J.* **77**, 1268–1283.
56. Powell, R. J., and Hildebrand, J. H. (1971) Diffusivity of helium-3, helium-4, molecular hydrogen, molecular deuterium, neon, methane, argon, krypton, and tetrafluoromethane in tri(perfluorobutyl)amine, *J. Chem. Phys.* **55**, 4715–16.
57. Hildebrand, J. H., and Lamoreaux, R. H. (1974) Diffusivity of gases in liquids, *Proc. Natl. Acad. Sci. U.S.A.* **71**, 3321–4.
58. Prager, S., and Long, F. A. (1951) Diffusion of hydrocarbons in polyisobutylene, *J. Am. Chem. Soc.* **73**, 4072–4075.
59. Conradi, R. A., Hilgers, A. R., Ho, N. F. H., and Burton, P. S. (1992) The influence of peptide structure on transport across Caco-2 cells. II. Peptide bond modification which results in improved permeability., *Pharm. Res.* **9**, 435–439.
60. Burton, P. S., Conradi, R. A., Hilgers, A. R., Ho, N. F. H., and Maggiora, L. L. (1992) The relationship between peptide structure and transport across epithelial cell monolayers, *J. Controlled Release* **19**, 87–98.
61. Chikhale, E. G., Ng, K.-Y., Burton, P. S., and Borchardt, R. T. (1994) Hydrogen bonding potential as a determinant of the in vitro and in situ blood-brain barrier permeability of peptides, *Pharm. Res.* **11**, 412–419.
62. Stenberg, P., Luthman, K., and Artursson, P. (1999) Prediction of membrane permeability to peptides from calculated dynamic molecular surface properties [published erratum appears in *Pharm. Res.*, Aug 1999, **16** (8), 1324], *Pharm. Res.* **16**, 205–12.
63. Reynolds, J. A., Gilbert, D. B., and Tanford, C. (1974) Empirical correlation between hydrophobic free energy and aqueous cavity surface area., *Proc. Natl. Acad. Sci. U.S.A.* **71**, 2925–2927.
64. Chothia, C. (1974) Hydrophobic bonding and accessible surface area in proteins, *Nature (London)* **248**, 338–339.
65. Nozaki, Y., and Tanford, C. (1971) The solubility of amino acids and two glycine peptides in aqueous ethanol and dioxane solutions, *J. Biol. Chem.* **246**, 2211–2217.
66. Rose, G. D., Geselowitz, A. R., Lesser, G. J., Lee, R. H., and Zehfus, M. H. (1985) Hydrophobicity of amino acid residues in globular proteins, *Science* **229**, 834–838.
67. Walter, A., and Gutknecht, J. (1984) Monocarboxylic acid permeation through lipid bilayer membranes, *J. Membr. Biol.* **77**, 255–264.
68. Davis, S. S., Higuchi, T., and Rytting, J. H. (1974) in *Advances in Pharmaceutical Sciences*, pp 73–261, Academic Press, London.
69. Xiang, T.-X., and Anderson, B. D. (1999) Molecular dissolution processes in lipid bilayers: A molecular dynamics simulation, *J. Chem. Phys.* **110**, 1807–1818.
70. Madison, V., and Delaney, N. G. (1983) Thermodynamics of solvation for methylproline peptides, *Biopolymers* **22**, 869–877.
71. Toniolo, C., Palumbo, M., and Benedetti, E. (1976) On the oxy analogues to the 3→1 intramolecularly hydrogen-bonded peptide conformations, *Macromolecules* **9**, 420–424.
72. Aubry, A., Cung, M. T., and Marraud, M. (1985)  $\beta$ I- and  $\beta$ II-turn conformations in model dipeptides with the Pro-Xaa sequences, *J. Am. Chem. Soc.* **107**, 7640–7647.
73. Morton, R. A., and Danyluk, S. s. (1974) Cis–trans conformational dependence of the carboxylate pK in glycylsarcosine, *Can. J. Chem.* **52**, 2348–2352.
74. Mizushima, S., Shimanogouchi, T., Tsuboi, M., and Arakawa, T. (1957) Near-infrared spectra of compounds with two peptide bonds and the configuration of a polypeptide chain. VI. Further evidence of the internal hydrogen bonding and the estimation of its energy, *J. Am. Chem. Soc.* **79**, 5357–61.
75. Gerig, J. T. (1971) The effect of adjacent charges on the kinetics of rotation of the peptide bonds, *Biopolymers* **10**, 2435–2443.

BI026701L